MANAGEMENT OF A SOLAR PV-BES MICROGRID POWERED BY THREE-PHASE PARALLEL INVERTERS

Mrs. K. Ramya[1], K. Pavan Kumar[2] , G.Veera babu[3] , S.Srija[4]

[1]Assistant Professor, Department of EEE, Sree vahini institute of science and technology., Tiruvuru., NTR District., AP, India

[2,3,4] UG scholar students Sree vahini institute of science and technology, Tiruvuru, NTR District, AP, India

Abstract: This study introduces a three-phase microgrid design that operates in both grid-interfaced (GI) and freestanding (SA) modes, utilizing solar photovoltaic (PV) and battery energy storage (BES). Parallel connections are made between a BES, two solar PV arrays, and the point of common coupling (PCC). Current/power sharing is the form of control for the parallel voltage source converters (VSCs). When in SA mode, the VSC linked to BES functions as a grid forming inverter, maintaining the PCC voltage, while in GI mode it is programmed to send continuous power to the grid. Current-controlled mode is the default operation for VSCs linked to PVs. The active fundamental weight of load currents is estimated using a complex coefficient complex variable filter-based frequency locked loop (CCCVF-FLL). The phase of the load/grid voltages is estimated using the same FLL in order to synchronize the microgrid with the utility grid.

I. PREAMBLEMENT

The microgrid is a decentralized collection of electrical sources, energy storage devices, and loads that may operate in grid-interfaced (GI) or autonomous (SA) modes depending on technical or economic considerations. It is a self-sufficient energy system that serves a specific geographical area [1]. The installation of microgrids has increased as energy prices from distributed renewable sources such as solar, wind, biomass, and tidal have decreased. Surplus electricity may be sent into the grid to earn money.

The utility grid's power quality is declining as a result of the power converters that are used in practically all electrical equipment, both residential and commercial. electricity converters operate with reliability and efficiency because to advances in pulse width modulation (PWM) and control methods, but they still require pulsing electricity from the utility grid. Customers suffer from the effects of harmonics in the utility grid's voltages and currents. Increased losses, improper operation of delicate loads, communication and protection system malfunctions, and inefficient distribution system use are the results [2].

When in GI mode, the microgrid should run at unity power factor (UPF). To guarantee UPF operating of the microgrid, passive and active compensating techniques are applied. Interfacing inductors are employed with each dispersed source to suppress the harmonics present in the current waveforms, whereas RC filters are utilized to extenuate harmonics in voltage waveforms [2]. This study describes a microgrid setup that uses a single battery energy storage system to power many solar photovoltaic (PV) arrays (BES). A separate voltage source converter (VSC) connects the BES to the point of common coupling (PCC).

Because it is intermittent, the solar PV array is an unreliable power source. Nonetheless, it may be used with energy storage to provide stability and dependability to the microgrid in low-light situations. In this paper, a

BES is regarded as an energy storage device. When PV power is insufficient to fulfil the demand of the local load, the excess energy from the PV array is stored in the BES and consumed. When the system is in GI mode, the excess energy may be sent back into the grid.

The maximum power point (MPP) voltage (VMPP) is the voltage at which the maximum power (MPP) of a solar PV array may be extracted at a given temperature and solar insolation. The PV array's properties (I-V and P-V) are very non-linear. The PV array's voltage is kept constant at VMPP by means of the MPP tracking (MPPT) controllers. The literature has presented a number of MPPT strategies, including fuzzy logic, incremental conductance (INC), short-circuit current, open-circuit voltage, and perturb and observe (P&O) methods [3-5]. The operational voltage is slightly perturbed and the power is verified in the P&O based MPPT algorithm. In the event that the measured power exceeds the initial power, the voltage is perturbed either in the same direction or in the other direction.

A single PV plant might not be able to provide the necessary amount of power due to the rise in load demand. The limited area may prevent the PV plant from being expanded up further. Furthermore, considering dependability and cost, constructing a single inverter with a very high power rating might not be the ideal option. Therefore, in the case of dispersed solar PV plants, using parallel inverters is a better option. When compared to a single centralised source, it improves system reliability since the remaining (n-1) modules can continue to supply power to the local load in the event of an inverter failure [6]. A BES is linked straight to a VSC in this instance, and two solar PV systems are connected in parallel with different VSCs. In SA mode, the BES-VSC functions as a grid creating inverter [7].

The frequency locked loop (FLL) based on a complex coefficient complex variable filter (CCCVF-FLL) is utilised to estimate the reference phase currents of VSCs linked to solar PVs [8]. Grid and PCC voltage frequency and phase are likewise estimated using the same FLL. An extra degree of flexibility is added to the basic FLL structure by the CCCVF-FLL. The extra degree of freedom improves the dynamic performance without materially impairing the FLL's capacity to filter.

II. System Design

The microgrid's architecture is illustrated in Figure 1. It is made up of a three-phase utility grid, two solar PV arrays connected to PCC via their VSCs, a boost converter with MPPT control, a BDC, a solid-state switch, and local loads. Load 1 is nonlinear, but Load 2 is inductive. Solid-state switches are used to control grid interruptions and reconnection. On both the grid and the load sides, RC filters are used to filter out voltage ripples and provide a channel for unexpected interruptions of current due to the source's inductive resistance.

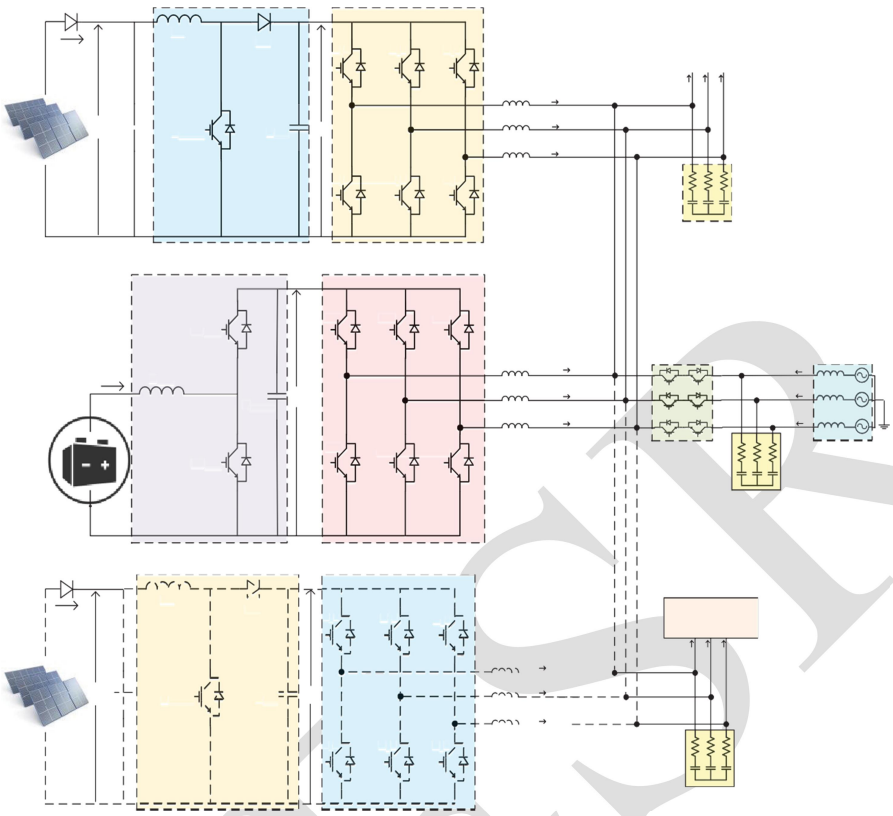

Fig : 1 MPPT Control Boost Converter; PV-VSC2 Voltage Source Converter

To collect the maximum power of the PV array, the boost converter linked to it is regulated using a P&O-based MPPT algorithm.

One of the important features of the microgrid is that the BES is linked to the three phase AC bus separately via a VSC, allowing it to act as a grid forming inverter in SA mode. Furthermore, the PV-VSC switch rating might be determined only on the basis of maximum PV power. This would improve the system's reliability and robustness. The BES may be utilized with several PV arrays.

Second, the same FLL is used to estimate phase and frequency components as well as load currents for PV-VSC control. It makes implementation easy.

III. Utilise Control Techniques

Both PV-VSCs run in current-controlled mode. In the GI state, the BES-vsc operates in current-controlled mode, whereas in the SA state, it operates in voltage-controlled mode. The boost converter ensures the maximum power tracking of the PV array by keeping the Vpv at VMPP. The BDC regulates the BES's charging and discharging currents as well as the BES-VSC's DC connection. The sections that follow provide a detailed explanation of each control approach.

A. MPPT control

To extract the most power from the PV array, whether in SA or GI mode, the voltage across it must be kept at

VMPP. This is accomplished by implementing the MPPT algorithm to control the boost controller. The controller produces a reference voltage (VPV*). The boost converter's duty signal is supplied by:

$$d = \frac{V_{Pv}^*}{V_{DC}^*} \qquad 1$$

The duty signal is compared to a saw tooth carrier to create the boost converter's switching pulses.

B. Controlling PV-VSC systems:

The PV-VSCs are operated the same way in both GI and SA modes. The surgery is depicted in Figure 2. The primary control stages are described as follows:

a) PCC Voltage Amplitude and Unit Templates:

The voltage amplitude at the PCC is expressed as [2]

$$V_t = \sqrt{\frac{2}{3}(V_{la}^2 + V_{lb}^2 + V_{lc})} \qquad 2$$

Where vla, vlb, and vlc are the voltages in the load phase. The in-phase unit templates are presented as follows:

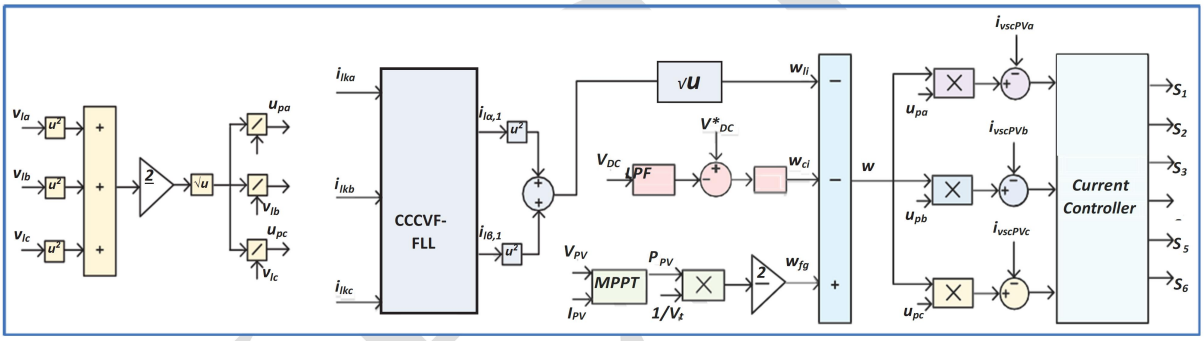

Fig : 2 PV-VSC management

$$u_{ia} = \frac{v_{la}}{V_t}, u_{ib} = \frac{v_{lb}}{V_t}, u_i = \frac{v_{lc}}{V_t} \qquad 3$$

b) Calculating the fundamental active weight of load currents: Figure 3 shows the construction of a complex coefficient complex variable filter-based FLL (CCCVF-FLL). First, the α and β components of load phase currents are determined using the Clarke's transformation:

$$\begin{bmatrix} i_{l\alpha} \\ i_{l\beta} \end{bmatrix} = \frac{1}{3}\begin{bmatrix} 2 & -1 & -1 \\ 0 & \sqrt{3} & -\sqrt{3} \end{bmatrix}\begin{bmatrix} i_{l1a} \\ i_{l1b} \\ i_{l1c} \end{bmatrix} \qquad 4$$

To compute the error in the α and β components of load phase currents (e_α and e_β), ilα and $i_{l\beta}$ are compared to the estimated components ($i_{l\alpha,1}$ and $i_{l\beta,1}$). $i_{l\alpha,1}(n)$ and $i_{l\beta,1(}n)$ are produced from Eqs.(7) and (8) by adding a unit delay to $i_{l\alpha,1}(n+1)$ and $i_{l\beta,1}(n+1)$.

$$e_{l\alpha(n)=i_{l\alpha}(n)-i_{l\alpha,1}(n)} \qquad 5$$

$$e_{l\beta(n)=i_{l\beta}(n)-i_{l\beta,1}(n)} \qquad 6$$

$$i_{l\alpha,1}(n+1) = ke_{l\alpha}(n) - ke_{l\beta}(n) - \omega_{il}(n)i_{l\beta,1}(n) \qquad 7$$

$$i_{l\beta,1}(n+1) = ke_{l\beta}(n) - ke_{l\alpha}(n) - \omega_{il}(n)i_{l\alpha,1}(n) \qquad 8$$

The estimated angular frequency, ωil(n), is determined from Eq. (9) by adding a unit delay to ωil(n+1), which is given by:

$$\omega_{il}(n+1) = \frac{\lambda}{I^2}\left(i_{l\alpha,1}(n)e_{l\beta}(n) - i_{l\beta,1}(n)e_{l\alpha}(n)\right) \quad 9$$

The fundamental active weight of load current (I) is given by λ=83540.

$$w_{li}(n) = I = \sqrt{i^2_{l\alpha,1}(n) + i^2_{l\beta,1}(n)} \quad 10$$

c) Active Loss Component Computation: For MPPT operation, the DC-link of PV-VSC must be controlled. The measured DC-link voltage is compared to the reference voltage, and the error (Verr) is sent to a proportional-integral (PI) controller. The output of the PI controller may be expressed as:

$$w_{ci}(n+1) = w_{ci}(n) + K_{pd}\left(v_{err}(n+1) - V_{err}(n)\right) + K_{id}\left(V_{err}(n+1)\right) \quad 11$$

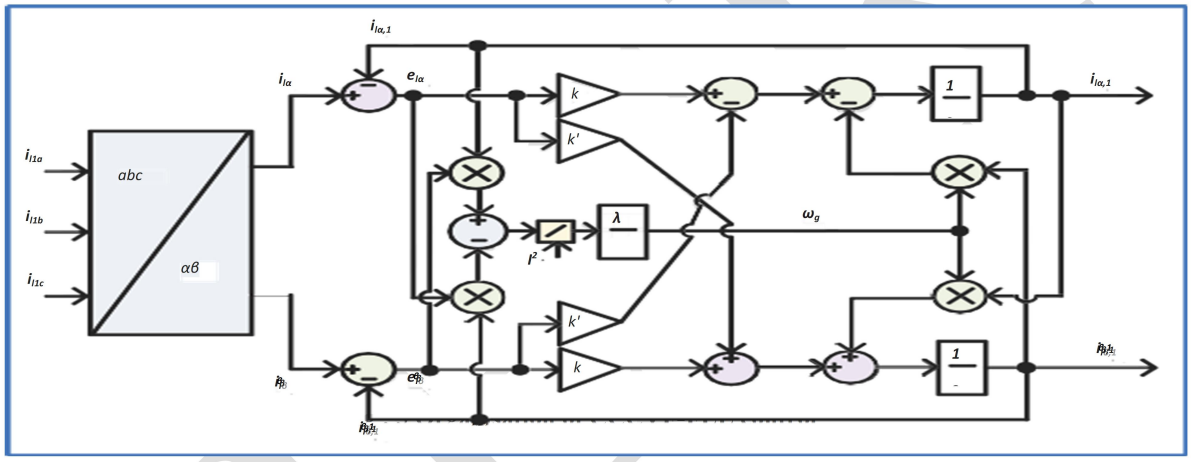

d. Feed-forward component computation: the PV array's excess electricity is delivered to the utility grid in GI mode and fed into the battery in SA mode. The weight for the feed-forward component is determined by:

$$w_{fg}(n) = \frac{2P_{pv}(n)}{3V_t} \quad 12$$

e. Estimation of Reference Currents: PV-VSC1 reference currents are calculated using the net active weight w(n) from Eq. (13).

$$w(n) = w_{fg}(n) - w_{li}(n) - w_{ci}(n) \quad 13$$

The reference phase currents are determined by multiplying the unit templates by the net active weight. They are stated as:

$$i_a^* = wu_{ia}, i_b^* = wu_{ib,} i_c^* = wu_{ic} \quad 14$$

f. Generation of Switching Pulses: Errors in PV-VSC1 currents are calculated by comparing measured currents (i_{1a}, i_{1b}, i_{1c}) to reference currents (i_a^*, i_b^*, i_c^*). The hysteresis controllers generate switching pulses for the

PV-VSC1 using the error signals. The same techniques are used to create the reference currents for the PV-VSC2.

C. BES-VSC control

Figure 4 demonstrates the BES-VSC's control of both GI and SA modes. The primary control steps are mentioned below:

1) GI mode operating of microgrids:

Microgrid operation in GI mode aims to maintain the UPF and provide consistent power to the grid.The weight for the feed-forward component is determined by:

$$w_{const}(n) = \frac{2P_{const}}{3V_t} \quad 15$$

To calculate the reference currents ($i^*_{ga}, i^*_{gb}, i^*_{gc}$), multiply the in-phase unit templates by $w_{const.}$

$$i^*_{ga} = w_{const}u_{ia}, i^*_{gb} = w_{const}u_{ib}, i^*_{gc} = w_{const}u_{ic} \quad 16$$

Hysteresis controllers generate switching pulses based on error signals acquired by comparing reference currents to observed grid currents (i_{ga}, i_{gb}, and i_{gc}).

2) Microgrid operation using SA Mode

The BES-VSC is used as a grid-forming inverter in SA mode. The following equations are used to obtain the reference voltages:

$$v^*_{la} = V^*_t sin(\omega_0 t) \quad 17$$

$$v^*_{lb} = V^*_t sin(\omega_0 t - {}^{2\pi}/_{3}) \quad 18$$

$$v^*_{lc} = V^*_t sin(\omega_0 t + {}^{2\pi}/_{3}) \quad 19$$

Where $V^*_t$is the load's reference voltages ($v_{la}v_{lb}v_{lc}$) are compared to the reference phase voltages ($v^*_{la}, v^*_{lb}, v^*_{lc}$), and the error outputs are sent to the PI controlleres. The PI controller's measured phase currents of the load1 ($i^*_{la}, i^*_{lb}, i^*_{lc}$) and error outputs are sent into hysteresis controllers, which produce switching pulses.

D. Synchronization Control

During the microgrid's reconnection to the utility grid, check that the amplitude of the grid voltages, frequency, and phase difference between the grid voltages and load voltages are within allowed limits. Only when all requirements are met can synchronization occur. The CCCVF-FL control is used to calculate the frequency and phase of load and grid voltages.

a) Extraction of Grid Voltage Phase and Frequency: Grid voltages are sent into the CCCVF-FLL controller, which computes angular frequency and phase. The expression for calculating angular frequency is as follows:

$$\omega_g(n-1) = \frac{\lambda}{V^2}\left(v_{g\alpha,1}(n)e_{g\beta}(n) - v_{g\beta,1}(n)e_{g\alpha}(n)\right) \quad 20$$

$v_{g\alpha,1}(n)$ and $v_{g\beta,1}(n)$ are the estimated α and β components of grid voltages, respectively. $e_{g\alpha}(n)$ and $e_{g\beta}(n)$ are the errors obtained by comparing $v_{g\alpha,1}(n)$with$v_{g\alpha}$(n) and $v_{g\beta,1}$ (n) with $v_{g\beta}$)(n). V is the amplitude of the estimated grid voltages, which is given by:

$$V = \sqrt{v_{g\alpha,1}^2(n) + v_{g\beta,1}^2(n)} \quad 21$$

A unit delay is applied to ωg(n+1) to obtain ωg(n). The formula for calculating the grid frequency fg(n) is given by:

$$f_g(n) = \frac{\omega_g(n)}{2\pi} \quad 22$$

To extract the phase, use the following expression:

$$\phi_g = cos^{-1}\left[\frac{v_{g\alpha,1}}{V}\right] \quad 23$$

b) Phase and Frequency Extraction from Load Voltages: The load voltages are passed into the CCCVF-FLL, which calculates the angular frequency and phase. The formula for calculating angular frequency is given by:

$$\omega_1(n+1) = \frac{\lambda}{V_1^2}\left(v_{l\alpha,1}(n)e_{l\beta}(n) - v_{l\beta,1}(n)e_{l\alpha}(n)\right) \quad 24$$

Where $v_{l\alpha,1}(n)$ and $v_{l\beta,1}(n)$ are the estimated α and β components of load voltages, and $e_{l\alpha}(n)$ and $e_{l\beta}(n)$ are the errors produced by comparing $v_{l\alpha,1}(n)$with $v_{l\alpha}(n)$ and $v_{l\beta,1}(n)$ with $v_{l\beta}(n)$, respectively. The amplitude of the estimated load voltages (vl) is determined by:

$$V_1 = \sqrt{v_{l\alpha,}^2(n) + v_{l\beta,1}^2(n)} \quad 25$$

To obtain $\omega_1(n)$, $\omega_1(n+1)$ is delayed by one unit. The expression for determining the load frequency $f_l(n)$ is given by:

$$f_1(n) = \frac{\omega_1(n)}{2\pi} \quad 26$$

The phase is extracted using the phrase that follows:

$$\phi_t = cos^{-1}\left[\frac{v_{l\alpha,1}}{V_1}\right] \quad 27$$

E. Control of the BDC

The BDC regulates the BES-VSC DC-link. It also regulates the charging and discharging current of the BES. It functions as a boost converter while discharging and a buck converter when charging. The observed DC-link voltage vdc batt is compared to the reference DC-link voltage $V_{DC\ batt}$ batt to determine the battery reference current, I_b^*.

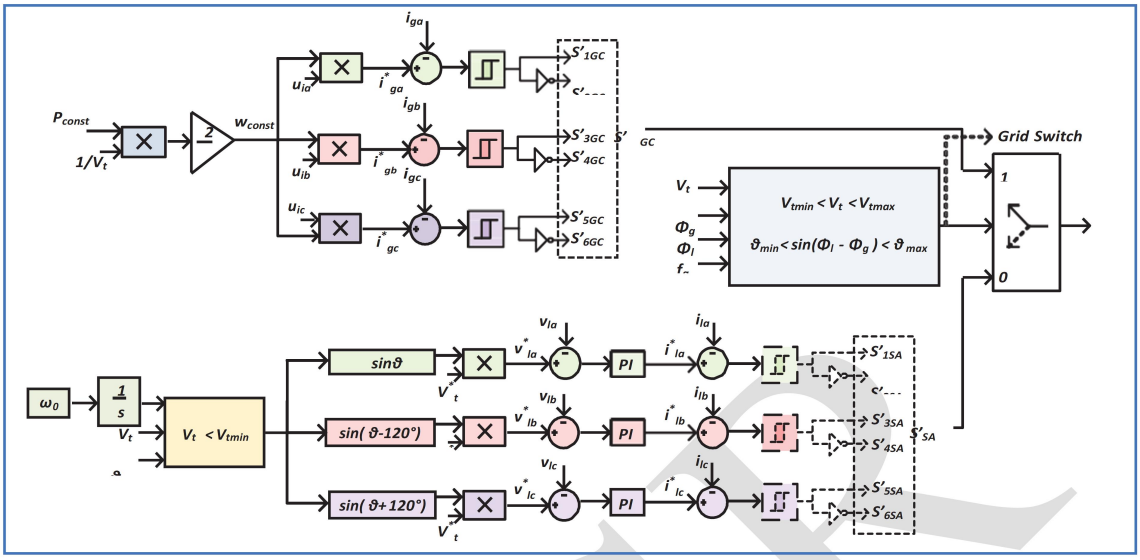

Fig : 4 BES-VSC and synchronisation management

The difference between I* and measured battery current (I) is sent into another PI controller to create the duty signal. The duty signal is compared to a saw-tooth carrier to provide PWM signals for the BDC switches. Figure 5 shows the BDC control.

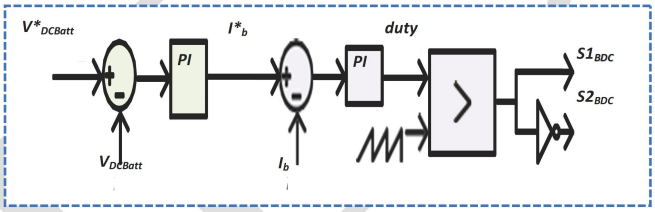

Fig : 5 BDC management

The system is simulated using the MATLAB/Simulink 2021b platform, and its functioning is examined in various circumstances.

IV Results and discussions

A. System performance in GI mode with different levels of solar insulation

Figure 6 displays system performance as solar insolation levels fluctuate. Figure 6 depicts grid voltages (vg) and currents (ig), load voltages (vl) and currents (il1 and il2), DC-link voltages of PV-VSC1 (VDC1) and PV-VSC2 (VDC2), grid power (Pgrid), PV power (PPV1 and PPV2), battery power (PBatt), and load power (PLoad1 and PLoad2). The solar insolation for PV1 decreases at 0.32s, as seen by the decrease in PPV1. As solar insolation drops, more power is pulled from the battery to meet load demands, while the grid is supplied with steady electricity. Because the voltages and currents are 180° apart, electricity is streaming into the grid. The DC-link of both PV-VSCs is controlled at 750V.

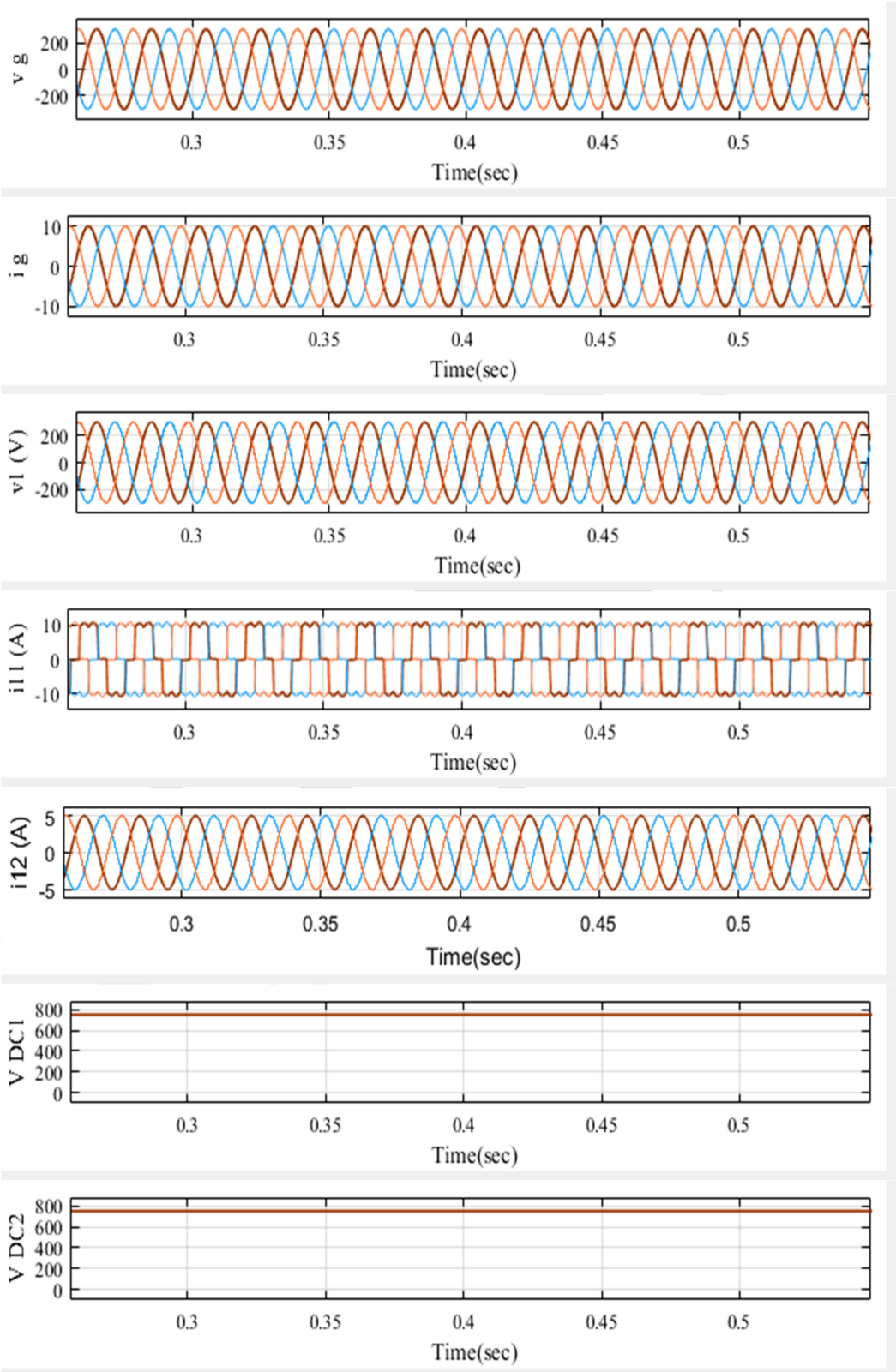
v g
200
0
-200
0.3
0.35
0.4
0.45
0.5
Time(sec)
i g
10
0
-10
0.3
0.35
0.4
0.45
0.5
Time(sec)
vl (V)
200
0
-200
0.3
0.35
0.4
0.45
0.5
Time(sec)
i11 (A)
10
0
-10
0.3
0.35
0.4
0.45
0.5
Time(sec)
i12 (A)
5
0
-5
0.3
0.35
0.4
0.45
0.5
Time(sec)
V DC1
800
600
400
200
0
0.3
0.35
0.4
0.45
0.5
Time(sec)
V DC2
800
600
400
200
0
0.3
0.35
0.4
0.45
0.5
Time(sec)

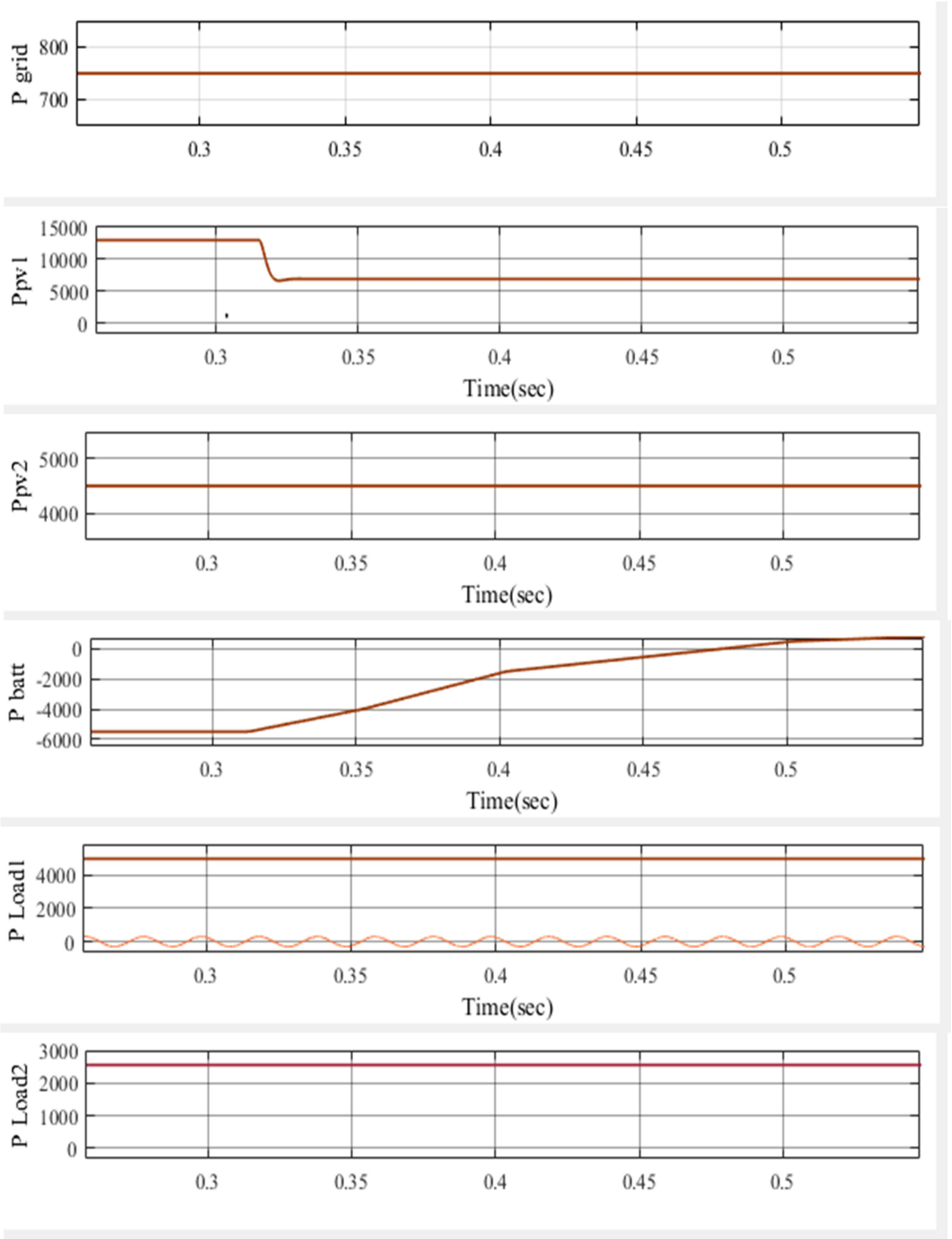

Fig : 6 System performance in GI mode as the amount of solar insolation fluctuates

B. Performance of Load Unbalancing in GI Mode

Figure 7 demonstrates system performance in GI mode during load unbalancing. Figure 7 shows vg, ig, vl, il1, il2, VDC1, VDC2, Pgrid, PPV1, PPV2, PBatt, PLoad1, and PLoad2. Load unbalancing is simulated by disconnecting 'a' phase load1 for 0.625s. The grid currents remain undistorted over the whole operating range. As the load demand decreases due to the disconnection of the 'a' phase load, the PV array's surplus power is

delivered to the battery. During load unbalancing, VDC1 remains within 10% of the required voltage and returns to normal after 6 fundamental cycles. The phase 'a' load is reconnected after 0.8 seconds.

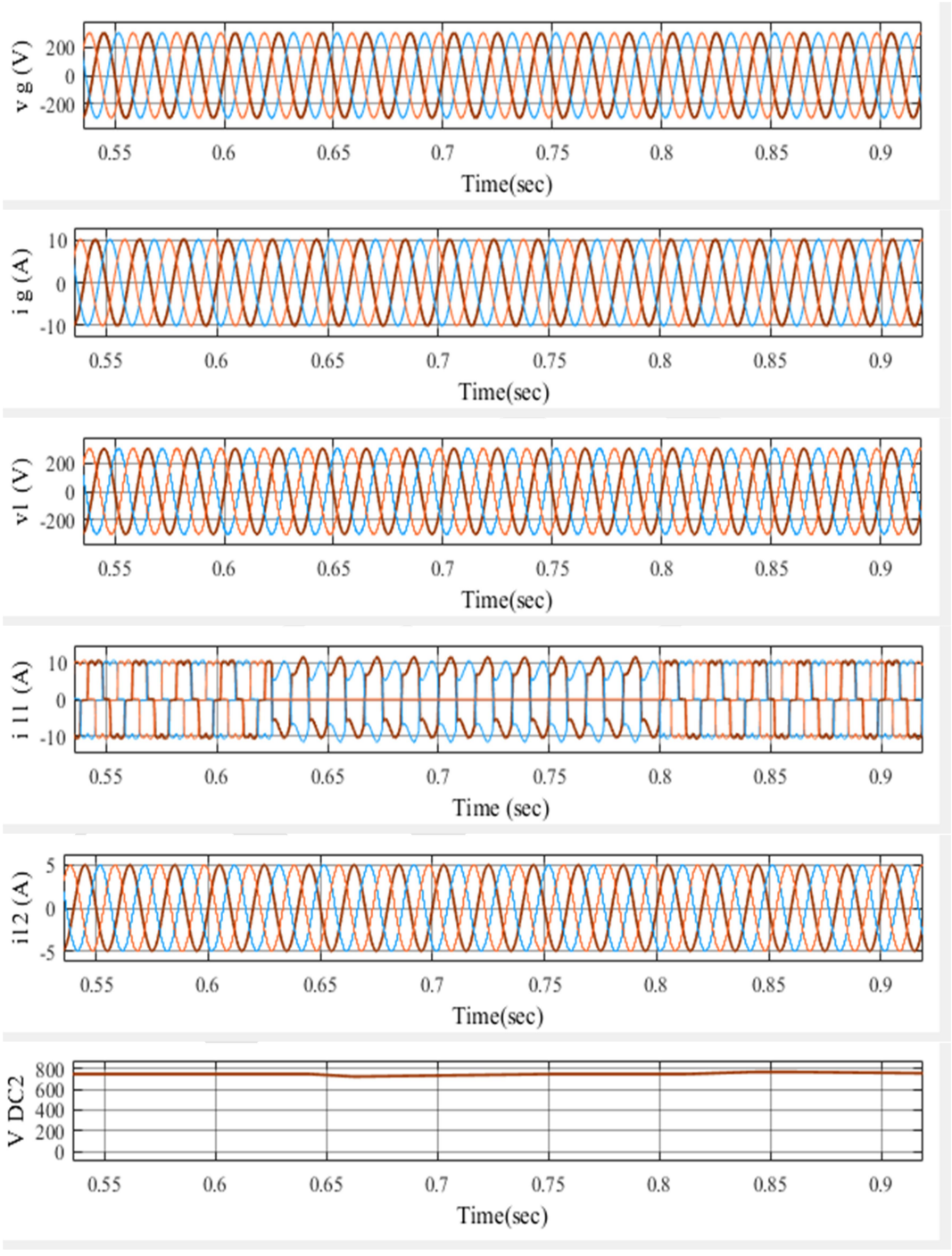

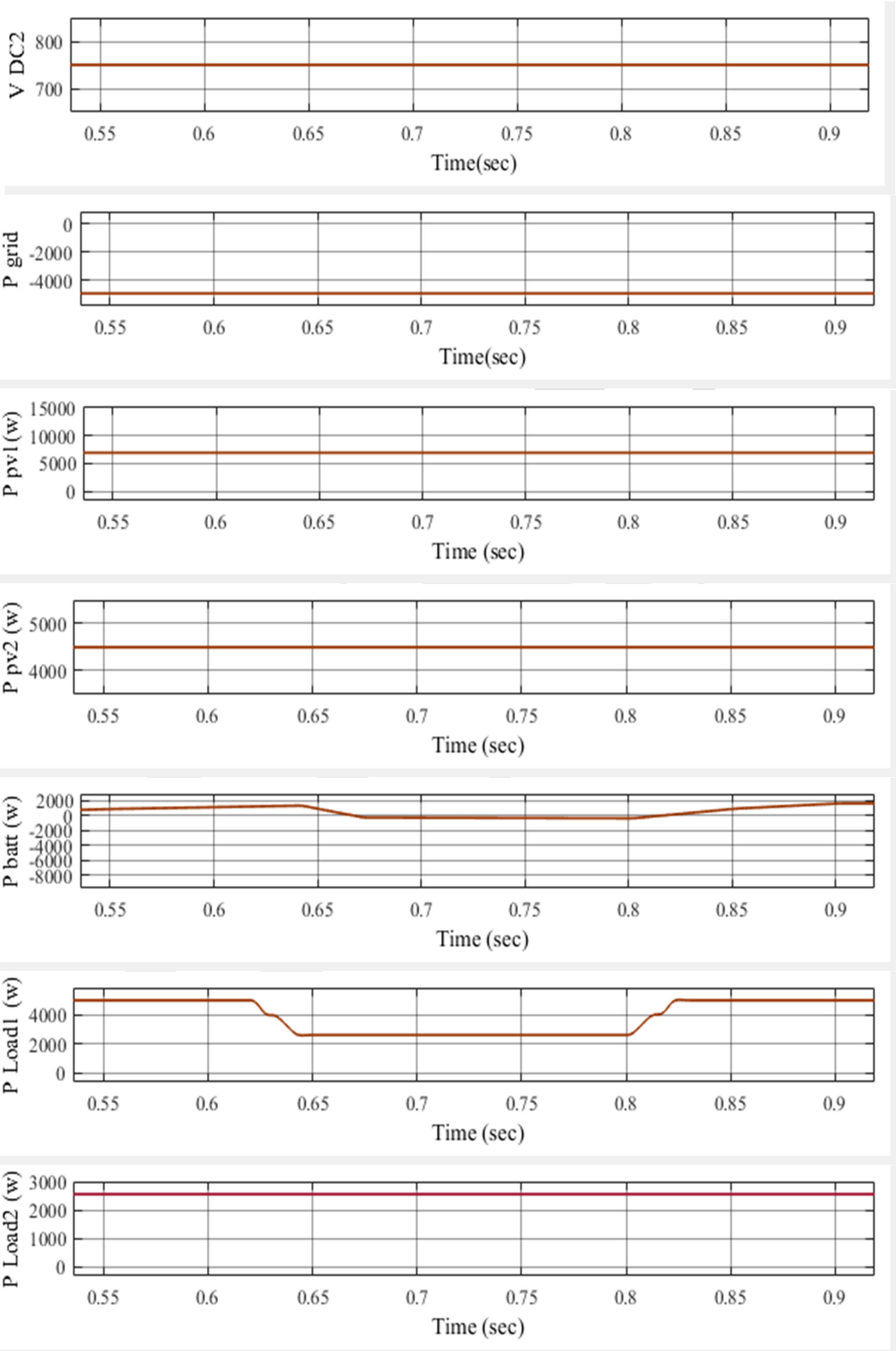
V DC2
800
700
0.55 0.6 0.65 0.7 0.75 0.8 0.85 0.9
Time(sec)
P grid
0
-2000
-4000
0.55 0.6 0.65 0.7 0.75 0.8 0.85 0.9
Time(sec)
P pv1 (w)
15000
10000
5000
0
0.55 0.6 0.65 0.7 0.75 0.8 0.85 0.9
Time (sec)
P pv2 (w)
5000
4000
0.55 0.6 0.65 0.7 0.75 0.8 0.85 0.9
Time (sec)
P batt (w)
2000
0
-2000
-4000
-6000
-8000
0.55 0.6 0.65 0.7 0.75 0.8 0.85 0.9
Time (sec)
P Load1 (w)
4000
2000
0
0.55 0.6 0.65 0.7 0.75 0.8 0.85 0.9
Time (sec)
P Load2 (w)
3000
2000
1000
0
0.55 0.6 0.65 0.7 0.75 0.8 0.85 0.9
Time (sec)

Fig : 7 Effectiveness of the GI micro grid

C. Change from GI to SA mode

Figure 8 displays system performance during the mode transfer from GI to SA. Figure 8 shows vg, ig, vl, il1, il2, VDC1, VDC2, PPV1, PPV2, PBatt, PLoad1 and PLoad2. The transition from GI to SA mode occurs in 1 second when the grid voltage falls below the permitted limit, indicating a defective grid. The transition from GI to SA is seamless, with no distortion in load voltages or currents. During SA mode, the BES-VSC acts as a grid-forming inverter, regulating the PCC voltages. During grid failures, grid currents decrease to zero, and the battery begins to charge using the PV array's surplus electricity.

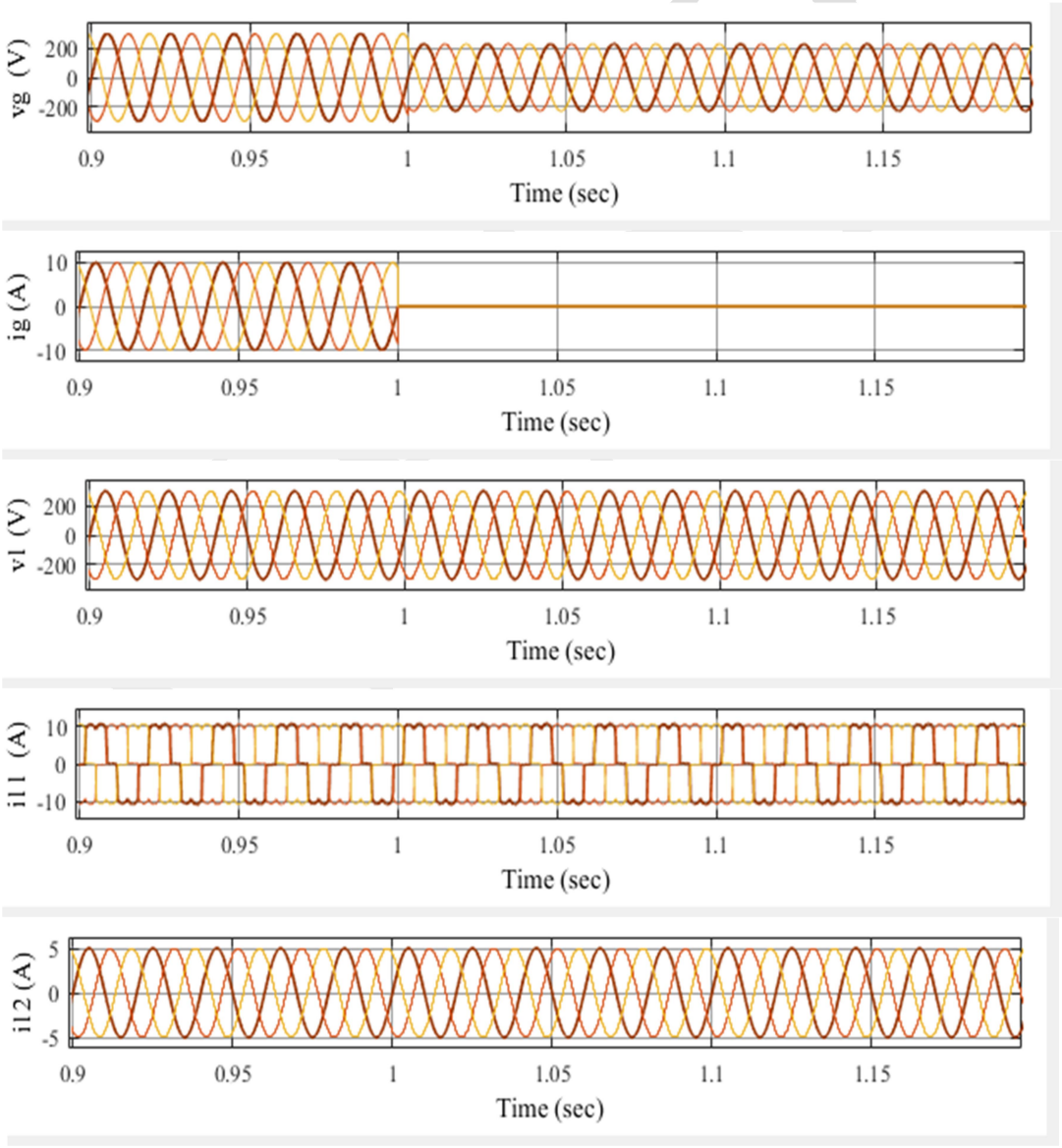

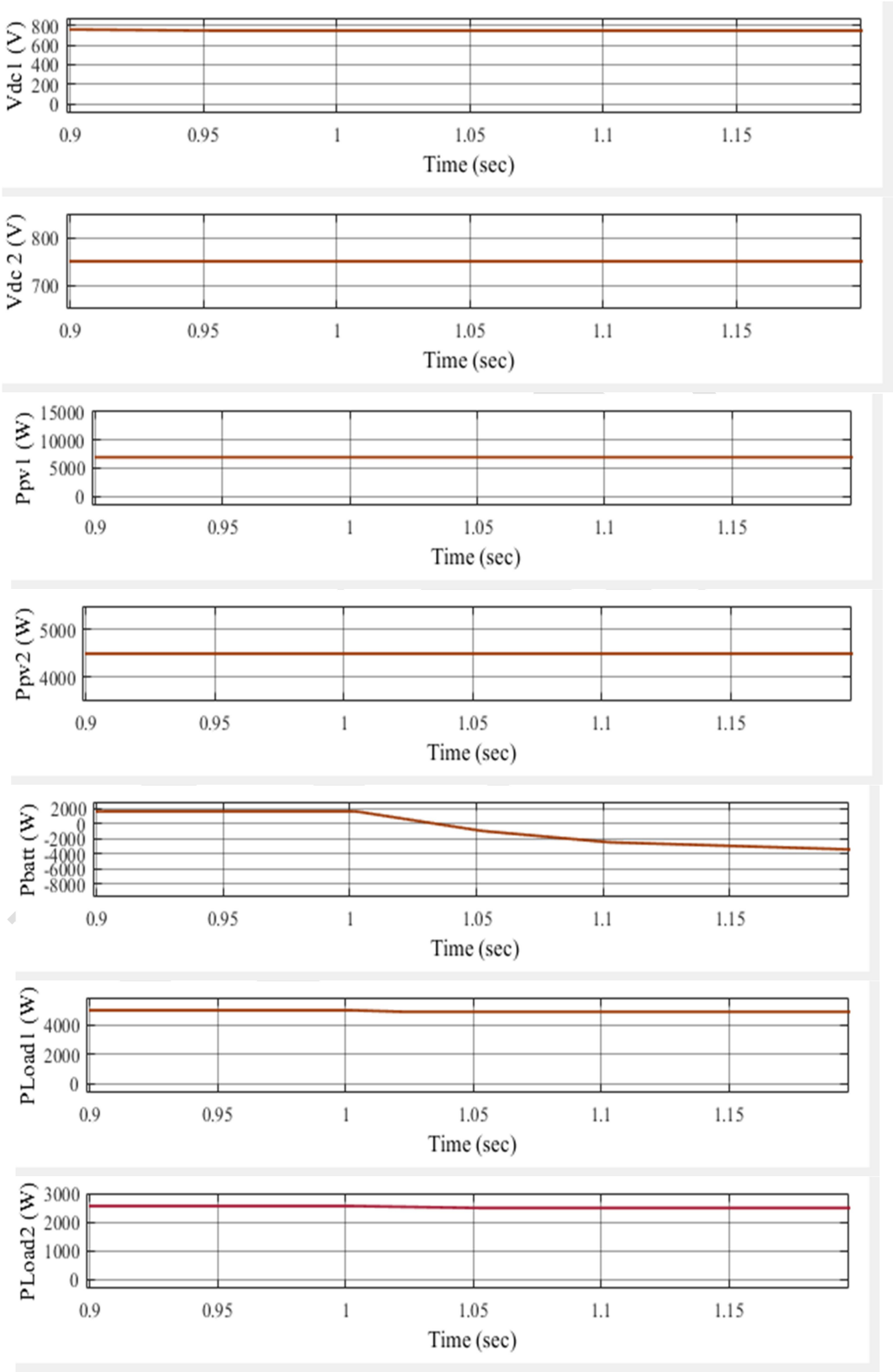
Vdc1 (V)
800
600
400
200
0
0.9
0.95
1
1.05
1.1
1.15
Time (sec)
Vdc 2 (V)
800
700
Time (sec)
Ppv1 (W)
15000
10000
5000
0
Time (sec)
Ppv2 (W)
5000
4000
Time (sec)
Pbatt (W)
2000
0
-2000
-4000
-6000
-8000
Time (sec)
PLoad1 (W)
4000
2000
0
Time (sec)
PLoad2 (W)
3000
2000
1000
0
Time (sec)

Fig : 8 Performance of the system when switching from GI to SA mode

D. System Performance under Changing Solar Insolation Levels in SA Mode

Figure 9 displays the system's performance in SA mode as the solar insolation level changes. Figure 9 depicts the variables vl, il1, il2, VDC1, VDC2, PPV1, PPV2, PBatt, PLoad1, and PLoad2. Solar insolation increases from 500W/m2 to 900W/m2 at 1.31s, as evidenced by a rise in PPV1 at that time. The battery charges at a greater pace. The load voltages and currents remain constant at both degrees of insolation.

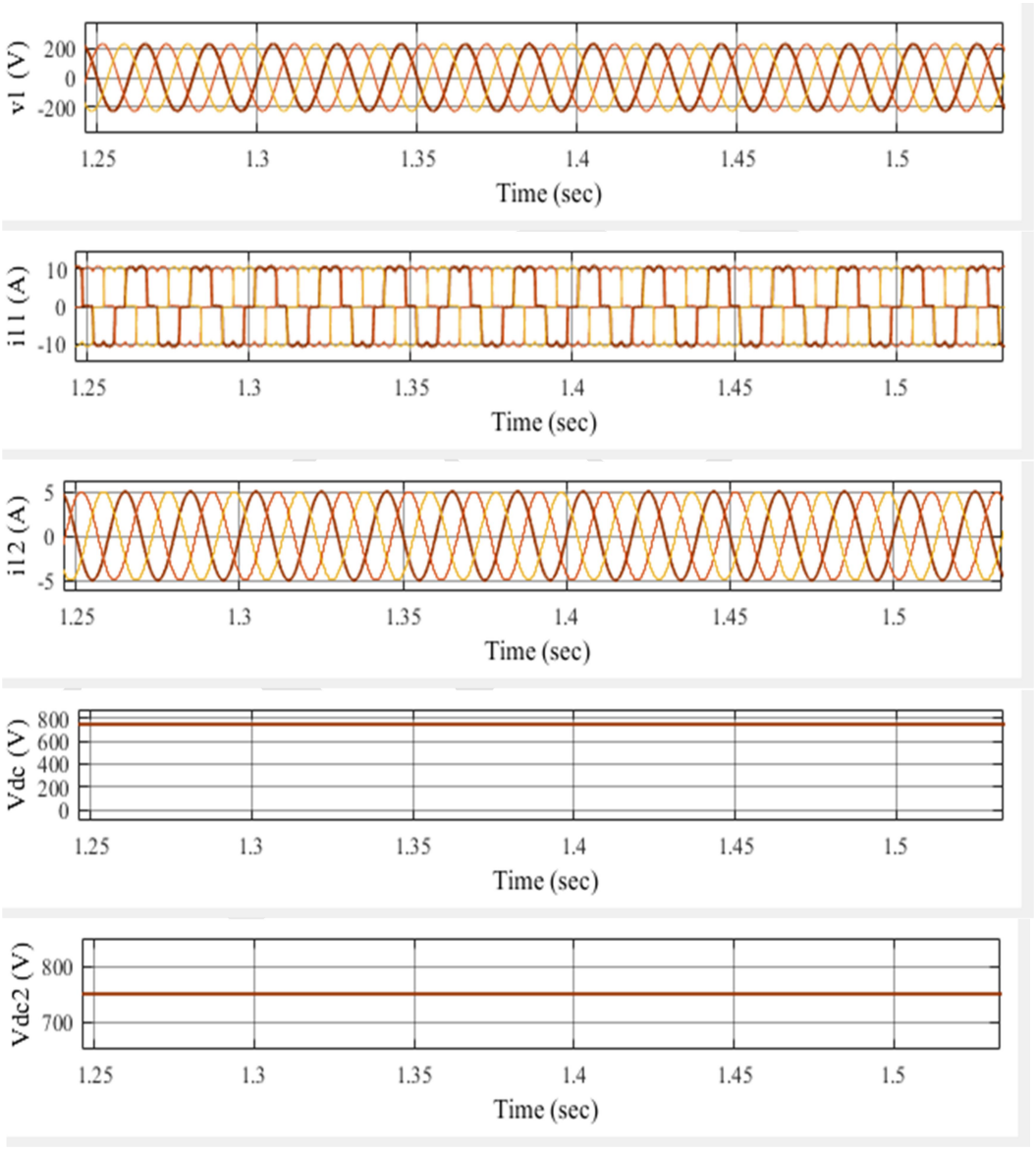

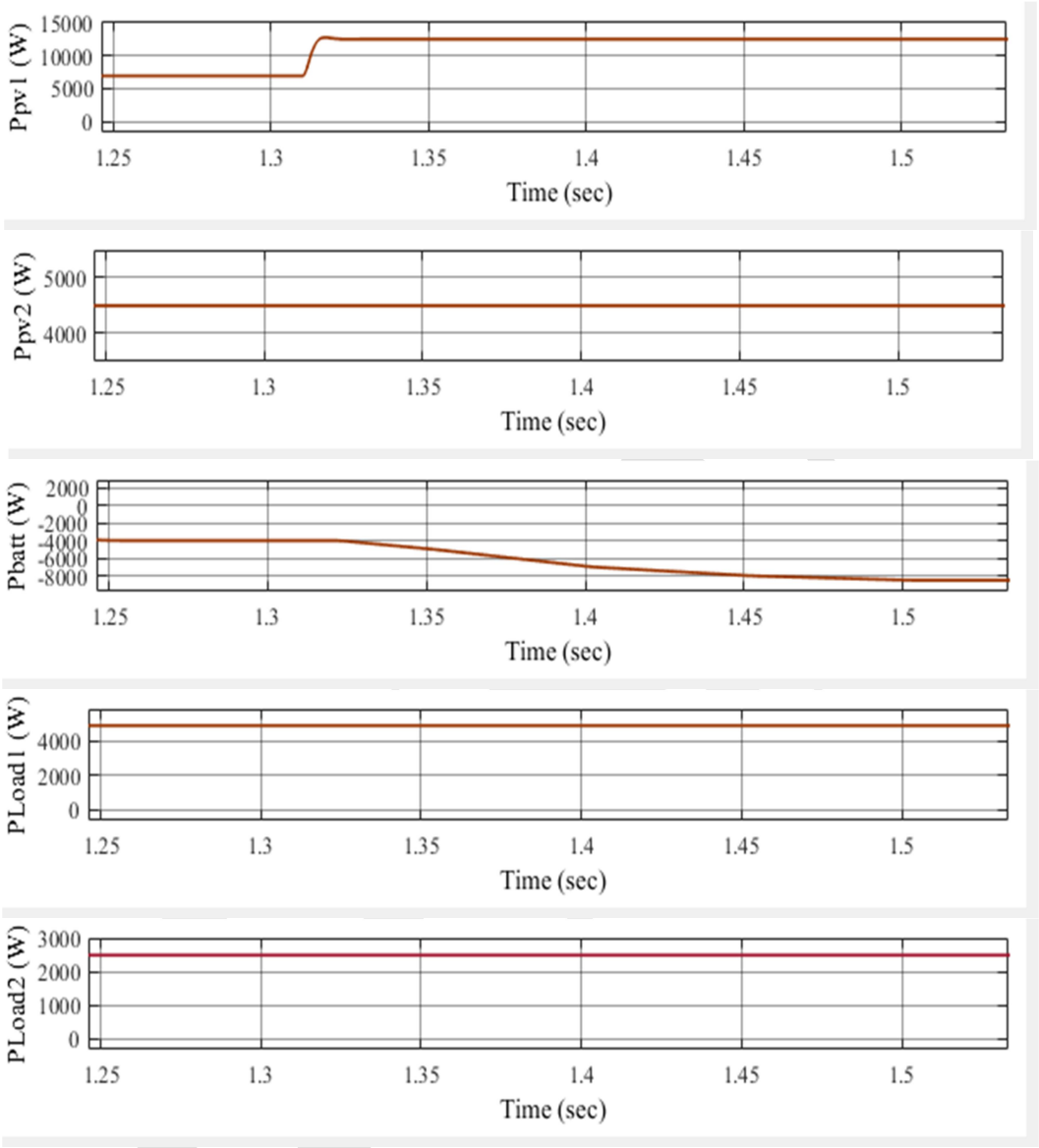

Fig : 9 system performance in SA mode as the amount of solar insolation varies

E. Function of Synchronization:

After the fault has been repaired, the microgrid is synced with the utility grid. Figure 10 demonstrates how the system performed during the microgrid's synchronization with the utility grid. Figure 10 displays the grid (ϕg) and load (ϕl) voltage phase angles, as well as grid switch locations. When grid voltages are restored to normal levels, the ϕl is matched with the ϕg. After matching ϕl and ϕg, the microgrid is synchronized with the utility grid. As a result, when the grid voltages are returned to normal, there is a delay in the operation of the grid switch.

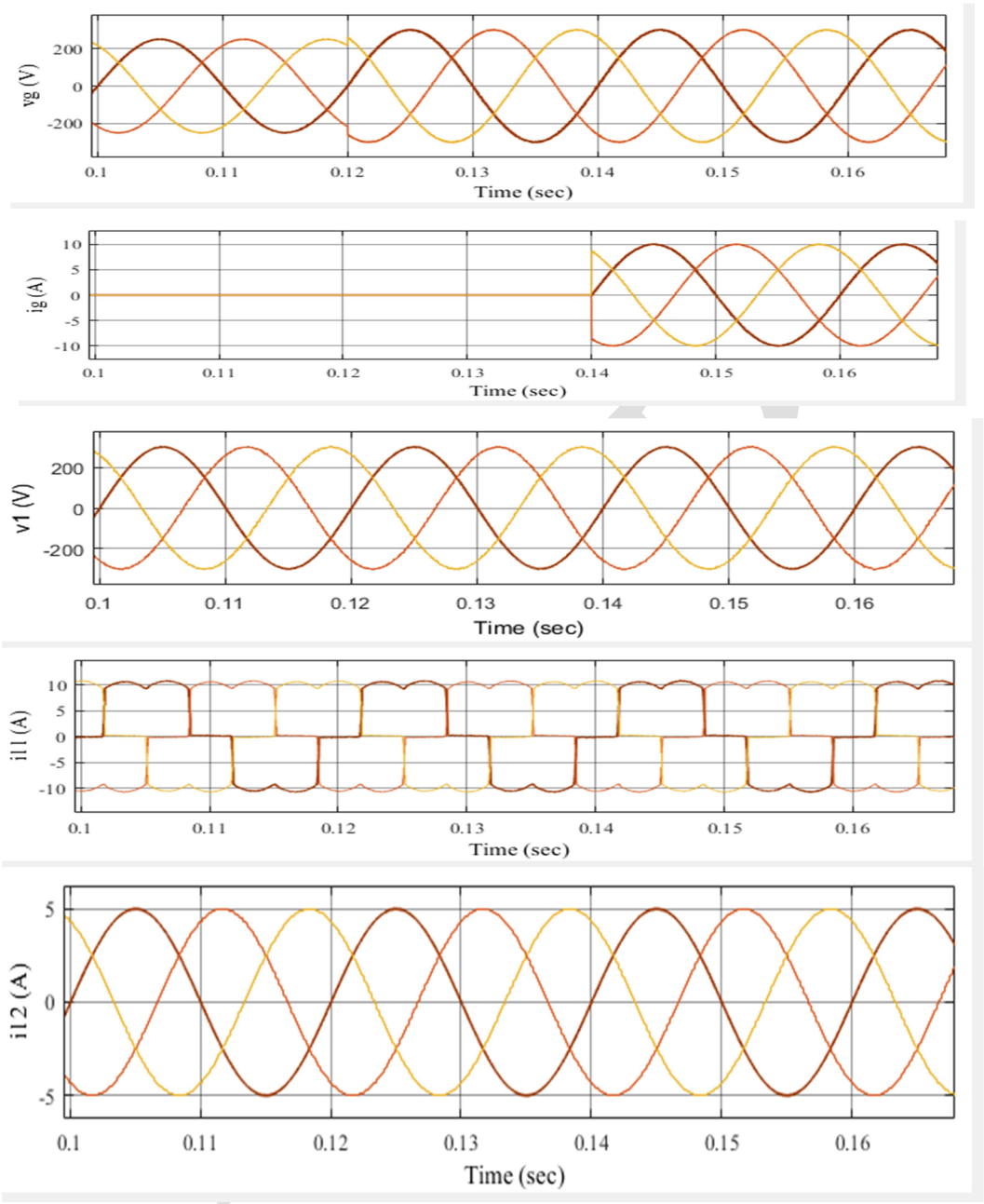

Fig : 10 synchronisation process

V. FINAL REPORT

This study investigates how the microgrid works in both GI and SA modes. The performance is investigated as the solar insolation and load unbalancing alter. The PV array always runs at MPP. Power balance is verified to meet all requirements. Power sharing between the PV arrays, BES, and load occurs under all operational situations. The CCCVF-FLL controller accurately estimates the phase and frequency of load and grid voltages.

The essential active weight of load currents is extracted using CCCVF-FLL for VSC operation, and it is found to perform better in power quality enhancement of microgrid.

REFERENCES

[1] "Microgrid defined: Three key features that make a microgrid a microgrid," Microgrid Knowledge. Available: https://microgridknowledge.com/microgrid-defined/.
[2] B. Singh, A. Chandra and K. Al-Haddad, Power Quality: Problems and Mitigation Techniques, Chichester, West Sussex, United Kingdom:Wiley, 2015.
[3] M. H. Reza and M. A. Shobug, "Efficiency evaluation of P&O MPPT technique used for maximum power extraction from solar photovoltaic system," IEEE Region 10 Symposium (TENSYMP), 2020, pp. 1808-181.
[4] E. Kim, M. Warner and I. Bhattacharya, "Adaptive step size incremental conductance based maximum power point tracking (MPPT)," 47th IEEE Photovoltaic Specialists Conf. (PVSC), 2020, pp. 2335-2339.
[5] M. L. Shah, A. Dhaneria, P. S. Modi, H. Khambhadiya and K. K. D, "Fuzzy logic MPPT for grid tie solar inverter," IEEE Inter. Conf. for Innovation in Tech. (INOCON), 2020, pp. 1-6.
[6] A. A. Khodadoost Arani and G. B. Gharehpetian, "A new control method for improving transient response of parallel VSIs in islanded microgrids," Smart Grid Conf. (SGC), 2014, pp. 1-5.
[7] D. Sharma, F. Sadeque and B. Mirafzal, "Synchronization of inverters in grid forming mode," IEEE Access, vol. 10, pp. 41341-41351, 2022.
[8] S. Golestan, J. M. Guerrero, J. C. Vasquez, A. M. Abusorrah and Y. Al-Turki, "A study on three-phase FLLs," IEEE Trans. on Pow. Electron., vol. 34, no. 1, pp. 213-224, Jan. 2019

AUTHORS

K. Ramya obtained her Bachelor of Technology in Electrical and Electronics Engineering from Sree Rama institute of technology and science in the year 2012.she completed M. tech in Sree Rama institute of technology and science. Her areas of interests are Power Systems, Electrical Machines, Power Electronics and Devices, Electrical Circuits and Power system Analysis. Electronics and Devices.

k. Pavan Kumar obtained his Bachelor of Technology in Electrical and Electronics from JNTUK, Tiruvuru, Andhra Pradesh, India. His areas of interests are Power Systems, Electrical Machines, and Power Electronics and Devices.

G. Veera Babu obtained his Bachelor of Technology in Electrical and Electronics from JNTUK, Tiruvuru, Andhra Pradesh, India. His areas of interests are Power Systems, Electrical Machines, and Power Electronics and Devices.

S. Srija obtained her Bachelor of Technology in Electrical and Electronics from JNTUK, Tiruvuru, Andhra Pradesh, India. Her areas of interests are Power Systems, Electrical Machines, and Power Electronics and Devices.